

TIMESCALES OF DISK EVOLUTION AND PLANET FORMATION: HST, ADAPTIVE OPTICS, AND ISO OBSERVATIONS OF WEAK-LINE AND POST-T TAURI STARS

1

WOLFGANG BRANDNER^{2,3,4}, HANS ZINNECKER⁵, JUAN M. ALCALÁ⁶, FRANCE ALLARD⁷, ELVIRA COVINO⁶, SABINE FRINK⁸, RAINER KÖHLER⁵, MICHAEL KUNKEL⁹, ANDREA MONETI¹⁰, ANDREAS SCHWEITZER^{11,4}

²University of Hawaii, Institute for Astronomy, 2680 Woodlawn Dr., Honolulu, HI 96822, USA;
brandner@ifa.hawaii.edu

³University of Illinois at Urbana-Champaign, Department of Astronomy, Urbana, IL 61801, USA

⁴Visiting astronomer, Cerro Tololo Inter-American Observatory, NOAO, which are operated by AURA, Inc.,
under contract with the NSF

⁵Astrophysikalisches Institut Potsdam, An der Sternwarte 16, D-14482 Potsdam, Germany;
koehler@aip.de, hzinnecker@aip.de

⁶Osservatorio Astronomico di Capodimonte Napoli, Italy; jmae@cerere.na.astro.it, covino@astrna.na.astro.it

⁷CRAL, Ecole Normale Supérieure, 46 Allée d'Italie, Lyon, F-69364 France, Cedex 07; fallard@cral.ens-lyon.fr

⁸Center for Astrophysics & Space Sciences, University of California San Diego, La Jolla, CA 92037-0424,
USA; sabine@ucsd.edu

⁹Astronomisches Institut der Universität Würzburg, Am Hubland, D-97074 Würzburg, Germany;
Michael.Kunkel@skf.com

¹⁰IEM-CSIC, Serrano 121, 28006 Madrid, Spain; amoneti@isis.iem.csic.es

¹¹University of Georgia, Dept. of Physics & Astronomy and Center for Simulation Physics, Athens, GA
30602-2451, USA; andy@hobbes.physast.uga.edu

Draft version October 30, 2018

ABSTRACT

We present high-spatial resolution HST and ground-based adaptive optics observations, and high-sensitivity ISO (ISOCAM & ISOPHOT) observations of a sample of X-ray selected weak-line (WTTS) and post (PTTS) T Tauri stars located in the nearby Chamaeleon T and Scorpius-Centaurus OB associations. HST/NICMOS and adaptive optics observations aimed at identifying substellar companions (young brown dwarfs) at separations ≥ 30 A.U. from the primary stars. No such objects were found within 300 A.U. of any of the target stars, and a number of faint objects at larger separations can very likely be attributed to a population of field (background) stars. ISOCAM observations of 5 to 15 Myr old WTTS and PTTS in ScoCen reveal infrared excesses which are clearly above photospheric levels, and which have a spectral index intermediate between that of younger (1 to 5 Myr) T Tauri stars in Chamaeleon and that of pure stellar photospheres. The difference in the spectral index of the older PTTS in ScoCen compared to the younger classical and weak-line TTS in Cha can be attributed to a deficiency of smaller size (0.1 to 1 μm) dust grains relative to larger size ($\approx 5 \mu\text{m}$) dust grains in the disks of the PTTS. The lack of small dust grains is either due to the environment (effect of nearby O stars and supernova explosions) or due to disk evolution. If the latter is the case, it would hint that circumstellar disks start to get dust depleted at an age between 5 to 15 Myr. Dust depletion is very likely related to the build-up of larger particles (ultimately rocks and planetesimals) and thus an indicator for the onset of the period of planet formation.

Subject headings: circumstellar matter — stars: low-mass, brown dwarfs — planetary systems — stars: pre-main sequence — open clusters and associations: individual (Scorpius-Centaurus, Chamaeleon)

1. INTRODUCTION

In the solar system, the coplanarity of planetary orbits and their moons, and the preferentially prograde rotation direction led Kant (1755) to the suggestion that the solar system evolved out of a flattened, disk like structure (“Urnebel”). Kant also proposed that planetary systems similar to the solar system might be common around other stars. Two of the major observational breakthroughs in astronomy in the 1990s were the direct imaging detection of circumstellar disks around young stars in nearby star-forming regions with the Hubble Space Telescope (O’Dell

et al. 1993; McCaughrean & O’Dell 1996; Burrows et al. 1996), and the indirect detection of giant planets in close orbits around nearby stars (Mayor & Queloz 1995; Marcy & Butler 1996). These important observational findings provide strong support for Kant’s hypotheses. Still uncertain, however, are the timescales of disk evolution and the exact physical processes leading to the formation of giant and terrestrial planets.

Giant planets in the solar system possess a core of higher density material surrounded by a shell of metallic hydrogen and an outer atmosphere. According to one model, a

¹Based on observations with the NASA/ESA Hubble Space Telescope obtained at the Space Telescope Science Institute, which is operated by the Association of Universities for Research in Astronomy, Inc., under the NASA contract NAS5-26555, observations at the European Southern Observatory, La Silla, (ESO Prop ID 58.E-0169), and observations with ESA’s Infrared Space Observatory.

higher density (rocky) core with a mass of $\approx 10 M_{\oplus}$ has to form first, before noticeable amounts of nebular gas can be accreted by the proto-giant planet. Simulations indicate that at least 10^6 yr are necessary to form a $10 M_{\oplus}$ rocky core (Lissauer 1987), and that another 10^7 yr are required for the $10 M_{\oplus}$ core to accrete $300 M_{\oplus}$ of nebular gas. It is still unknown if massive circumstellar disks can indeed survive for such an extended period. A second model, recently reinstated by Boss (1998), suggests that gravitational instability of a protoplanetary disk leads directly to the formation of a giant gaseous protoplanet on time scales as short as 10^3 yr. The rocky core then forms due to the settling of dust grains initially acquired, and by further accretion of solid bodies in the course of the following 10^5 yr. The difference in timescales for the formation of giant planets in the two models provides observational means to decide for or against either model by studying the circumstellar environment of stars with ages ≤ 15 Myr.

Weak-line (WTTS) and the even more evolved post-T Tauri stars (PTTS) are prime targets since – contrary to the very young classical T Tauri stars – they lack strong 1.3 mm dust continuum emission. This suggests that WTTS (and PTTS) no longer possess massive cold circumstellar dust disks (Beckwith et al. 1990, Henning et al. 1993). In WTTS and PTTS, the (dusty) circumstellar matter was either already partially accreted onto the central star or redistributed to form planetesimals or – via disk fragmentation – to form directly giant planets.

We devised a twofold strategy in order to study disk evolution and the timescales of the formation of planetary systems. First, taking advantage of the high sensitivity of the Infrared Space Observatory (ISO, Kessler et al. 1996), we searched for evidence of circumstellar disks around the presumably diskless WTTS and PTTS. Secondly, using high-spatial resolution imaging, we aimed at directly detecting faint substellar companions to the WTTS and PTTS.

Section 2 describes the sample selection. In Section 3 we explain the observing strategies and give an overview of the data reduction and analysis. Section 4 describes the attempt to detect substellar companions using the NASA/ESA Hubble Space Telescope (HST) and ground-based adaptive optics (AO). The results of the ISO observations and their implications are discussed in Section 5. An overall summary of the findings is presented in Section 6.

2. SAMPLE SELECTION

2.1. Selection of star forming regions

We selected the nearby (≈ 150 pc) Chamaeleon T association and the Scorpius-Centaurus OB association for our study. Young low-mass stars in OB associations are of particular interest, as most stars – including our Sun (see Vanhalla 1998, and references therein) – are believed to have originated in OB associations (e.g., Miller & Scalo 1978). In the course of photometric and spectroscopic follow-up studies of ROSAT sources, an initial sample of about 150 young, X-ray active late-type stars was identified in the Chamaeleon T association (Alcalá et al. 1995, 1997; Covino et al. 1997) and the Scorpius-Centaurus OB association (Kunkel et al. 2000).

2.2. Classification of evolutionary status

Traditionally, ages for pre-main sequence stars are derived based on their location above the main-sequence and by comparison with theoretical evolutionary tracks and isochrones in an HR-diagram. This approach relies on precise distance estimates in order to derive luminosities. In ScoCen and Cha, however, parallax measurements are only available for a handful of the X-ray active low-mass stars (see Frink et al. 1998; Neuhäuser & Brandner 1998; Kunkel et al. 2000). Furthermore, the individual parallax measurements indicate a relatively large spread in distance among various members of these associations. Hence it would be advantageous to determine the evolutionary status of the X-ray active low-mass stars using properties which are independent of the distance, like, e.g., spectral features.

In general, the X-ray active low-mass stars in Chamaeleon exhibit higher lithium equivalent widths than their counterparts in Scorpius-Centaurus. As lithium is continuously destroyed near the bottom of the convection zone, the photospheric lithium abundance decreases with increasing stellar age (Herbig 1965; Bodenheimer 1965). Therefore the lower lithium abundance indicates that the low-mass stellar population in ScoCen is older than in Chamaeleon.

Martín (1997, 1998) suggested a refined classification, based on H α and lithium equivalent widths as a function of spectral type to distinguish between CTTS, WTTS and PTTS. In a diagnostic diagram, late-type PTTS occupy a region intermediate between WTTS and stars in young open clusters like the Pleiades or α Per with ages of 60 to 120 Myr. Unfortunately, the lithium criterion can only be applied to stars of spectral type K0 and later, and does not allow to discriminate pre-main-sequence from zero-age-main-sequence (ZAMS) stars of earlier spectral types. Thus the number of stars located in the PTTS region of the diagnostic diagram represents only a lower limit to the total number of PTTS in a stellar population (Martín 1997). Therefore additional criteria like stellar kinematics (e.g., Feigelson 1996; Frink et al. 1997, 1998) are needed in order to distinguish between pre-main-sequence and ZAMS stars of spectral type K0 and earlier.

In order to avoid a contamination of our sample by ZAMS field stars, unclassified stars according to the diagnostics by Martín (1997, 1998) were largely rejected. In Chamaeleon, the majority of the young late-type stars are CTTS and WTTS and have typical ages between 1 Myr and 5 Myr (Alcalá et al. 1995). In the Scorpius-Centaurus OB association, a total of 76 TTS were detected. 49 of them can be classified as PTTS, 20 as WTTS and 7 as CTTS. 42 X-ray active stars in ScoCen remain unclassified. Typical ages for the WTTS and PTTS in ScoCen are of the order of 5 Myr to 15 Myr (Kunkel et al. 2000).

The sample was narrowed down to about 50 WTTS and PTTS by selecting preferentially late-type stars with lithium equivalent width $\gtrsim 0.1$ to 0.6 \AA .

2.3. Preselection against binary systems

As we aimed for the search for faint (substellar) companions and the study of disk evolution, it is important to consider the effect of binary stars. In binary systems, the complex dynamics and gravitational interactions between the individual components and their circumstellar and circumbinary disks might influence the evolution of circum-

stellar disks and aggravate or even completely inhibit the formation of substellar companions (Papaloizou & Pringle 1977; Artymowicz & Lubow 1994). Recent observations of circumstellar disks in multiple systems support these theoretical predictions (e.g. HK Tau, Stapelfeldt et al. 1998, Koresko 1998; HV Tau, Monin & Bouvier 2000). All stars in the sample were therefore surveyed for visual and spectroscopic binary companions (Brandner et al. 1996; Covino et al. 1997; Köhler et al. 2000; Kunkel et al. 2000). None of the detected companions was faint enough to be classified as a substellar source. Binary and multiple systems with separations less than $3''$ (450 A.U. at a distance of 150 pc) were excluded from the final target list. Table 3 gives an overview on the physical properties of the stars which were observed with HST and ISO.

3. OBSERVATIONS AND DATA REDUCTION

3.1. *HST/NICMOS observations*

3.1.1. *Observing Strategy*

Young substellar companions are still relatively hot, and are thus considerably more luminous and much easier to spot than evolved (older and cooler) substellar companions (Brandner et al. 1997; Malkov, Piskunov, & Zinnecker 1998). Maybe somewhat counterintuitive is the fact that the best wavelength region to search for substellar companions is the near-infrared between $1\ \mu\text{m}$ and $2\ \mu\text{m}$. The spectral energy distribution of late-type dwarfs and thus of young brown dwarfs and giant planets is very peculiar (Allard & Hauschildt 1995; Burrows et al. 1997). The molecular opacities which globally define the continuum cause the spectral energy distribution to peak between $1\ \mu\text{m}$ and $2\ \mu\text{m}$, almost independently of the effective temperature. Using the HST/SYNPHOT simulator and “Intermediate model spectra” for brown dwarfs and low-mass stars from Allard et al. (1996), we simulated the expected brightness differences between a substellar companion with an effective temperature of 900 K, and its primary star with an effective temperature of 3800 K and 2800 K, respectively, when observed through various NICMOS filters (Table 1). The narrow-band F108N filter and the intermediate band F165M filter provide the smallest brightness difference between the primary and a substellar companion. For the HST observations we selected F108N because of its shorter wavelength which yields a 35% better spatial resolution compared to F165M. In addition, the narrowband F108N filter provides a monochromatic, very well defined diffraction pattern around the science target, which is rather independent of the color of the object. More recent evolutionary models for low-mass stars and “NextGen model spectra” (Allard et al. 1997, Baraffe et al. 1998, Hauschildt et al. 1999) largely confirm our choice of filter selection for the HST/NICMOS observations.

In order to minimize the brightness difference between the primary and any possible substellar companion even further, we selected M-type WTTS and PTTS because of their smaller intrinsic luminosity compared to earlier spectral type WTTS and PTTS. Simulations with the Tiny-Tim PSF simulator (Krist & Hook 1997) indicated that it would be possible to detect an object 5^{m} fainter than the primary at a separation of $0''.2$. At a distance of 150 pc, a separation of $0''.2$ corresponds to 30 A.U., i.e. comparable to the semimajor axis of Neptune’s orbit.

3.1.2. *Observations*

The NICMOS camera aboard HST was installed in February 1997 (Thompson et al. 1998). HST/NICMOS observations (see Table 2) of 24 M-type WTTS and PTTS in Chamaeleon and Scorpius-Centaurus were carried out between 1997 Aug 14 and Sep 22 using NICMOS camera 1 (NIC1, $0''.043/\text{pixel}$). The observations were obtained in the F108N filter using MULTIACCUM mode. 18 of the targets were also observed in the F110M filter in order to obtain additional color information. Exposure times were between 2560s to 3072s in F108N, and between 64s to 192s in F110M.

3.1.3. *Data reduction and analysis*

The data reduction was carried out using the IRAF/STSDAS package CALNICA V3.1. For the data reduction, we replaced the model dark frames (as provided by STScI) with darks derived from archived on-orbit measurements. The photometric accuracy of the flux measurements for the faint sources is limited by the uncertainties in the dark/bias subtraction, flatfield errors, and the resulting uncertainties in the local background. The overall photometric uncertainties are of the order of $0^{\text{m}}.05$ for the brighter objects, and $0^{\text{m}}.1$ to $0^{\text{m}}.2$ for the fainter sources. Figures 1 and 2 show examples of the reduced frames.

As the NICMOS PSF can vary significantly from one HST orbit to the next, the HST/NICMOS observations of all target stars were used to build up a library of HST/NIC1 PSFs in the F108N and F110M filters. For each set of observations, we then identified the best matching PSF in the library. Sub-pixel offsets between target and PSF were computed by cross-correlating the individual frames. The PSF was then Fourier-shifted, scaled, and subtracted. The resulting difference frames were searched for faint, close companions. Figure 4 shows the typical detection limit (solid line) in terms of brightness difference versus separation. It would have been possible to detect a $4^{\text{m}}.7$ fainter companion at a separation of $0''.2$, and a 8^{m} fainter companion at a separation of $1''$. This detection limit is in good agreement with the detection limit derived from the simulations based on TinyTim PSFs.

Three of the “single” stars turned out to be close binaries, and two of the three wide binaries turned out to be hierarchical triple systems (Figure 1). A number of faint objects, which were found close to some of the target stars, are shown in Figure 2.

3.2. *Adaptive Optics Observations*

The observing strategy for the adaptive optics observations with ADONIS/SHARP at the ESO 3.6m telescope was similar to that of the HST/NICMOS observations. Because of the need for a star sufficiently bright for wavefront sensing, only bright G- and K-type stars could be observed. The observations were carried out in the broadband H and K filter, with the intent to gather additional data with the circular variable filter (CVF) for good candidates for substellar companions.

In two observing nights in March 1997, a total of 17 WTTS and PTTS in Chamaeleon and Scorpius Centaurus were observed, and two 4^{m} to 5^{m} fainter companions were identified (RXJ 12253-7857 and RXJ 14150-7822, see

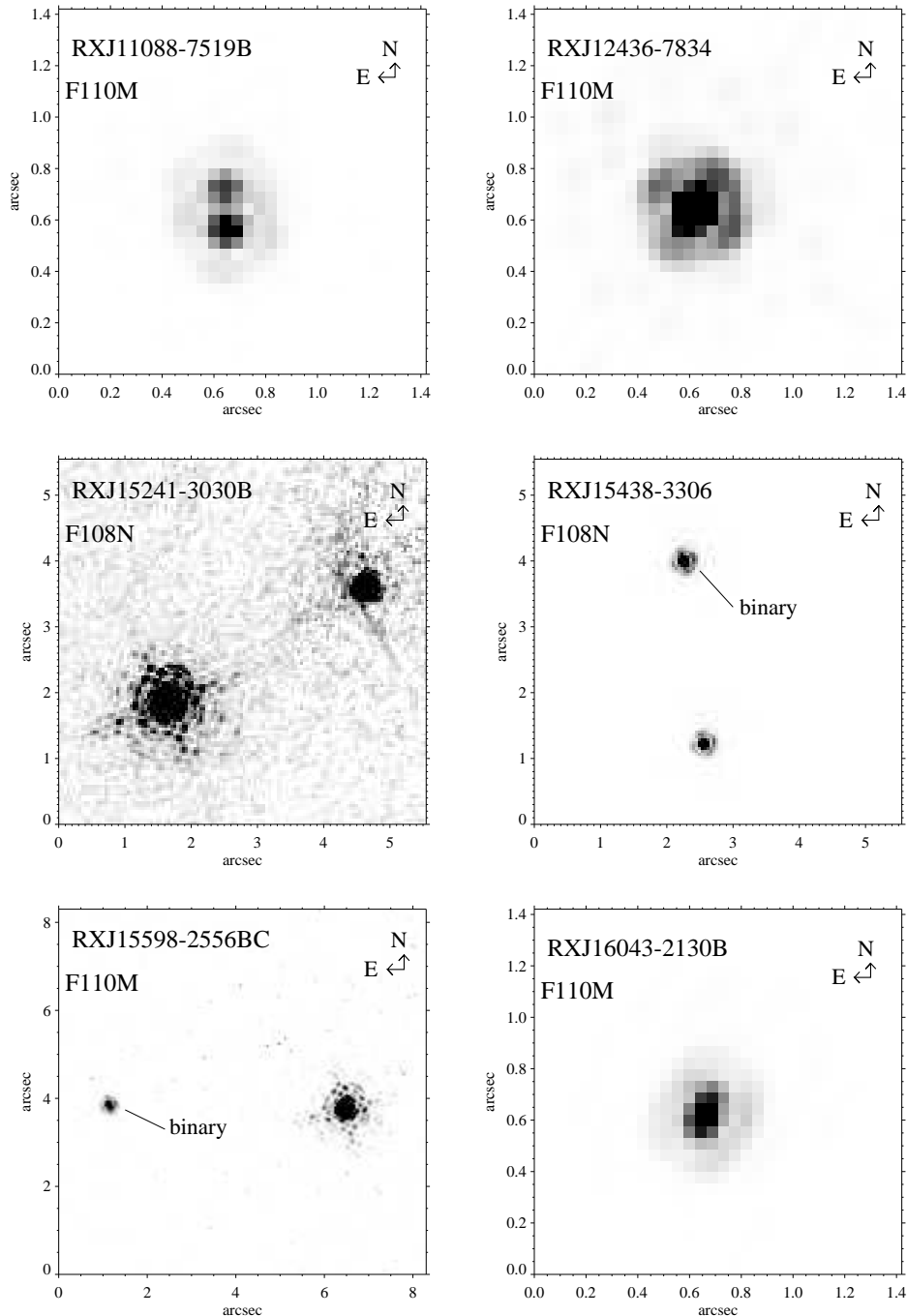


FIG. 1.— Finding chart for binary and triple systems. Two of the three wide binary systems in our survey turned out to be hierarchical triple systems (RXJ 15438-3306 and RXJ 15598-2335BC). North is up and east is to the left.

Brandner et al. 1997). Unfortunately, unfavorable weather conditions during the second half of the second observing night prevented any immediate follow-up using the CVF.

3.3. ISOCAM & ISOPHOT observations

3.3.1. Observing Strategy

ISO offered the unique opportunity to search for subtle infrared excesses from circumstellar disks and substellar companions with unprecedented sensitivity. As the temperature of circumstellar disks changes with radial dis-

tance from the star, one can probe the radial surface density and temperature profile of circumstellar disks by observing them at a wide range of wavelengths. If for example in the course of disk evolution the inner disk is depleted first, it should still be possible to detect the cooler, outer parts of the disk at longer wavelengths. Consequently, the observing strategy was to observe the sample stars both with ISOCAM (Césarsky et al. 1996) at $6.7 \mu\text{m}$ and $15 \mu\text{m}$, and with ISOPHOT (Lemke et al. 1996) at $60 \mu\text{m}$ and $90 \mu\text{m}$.

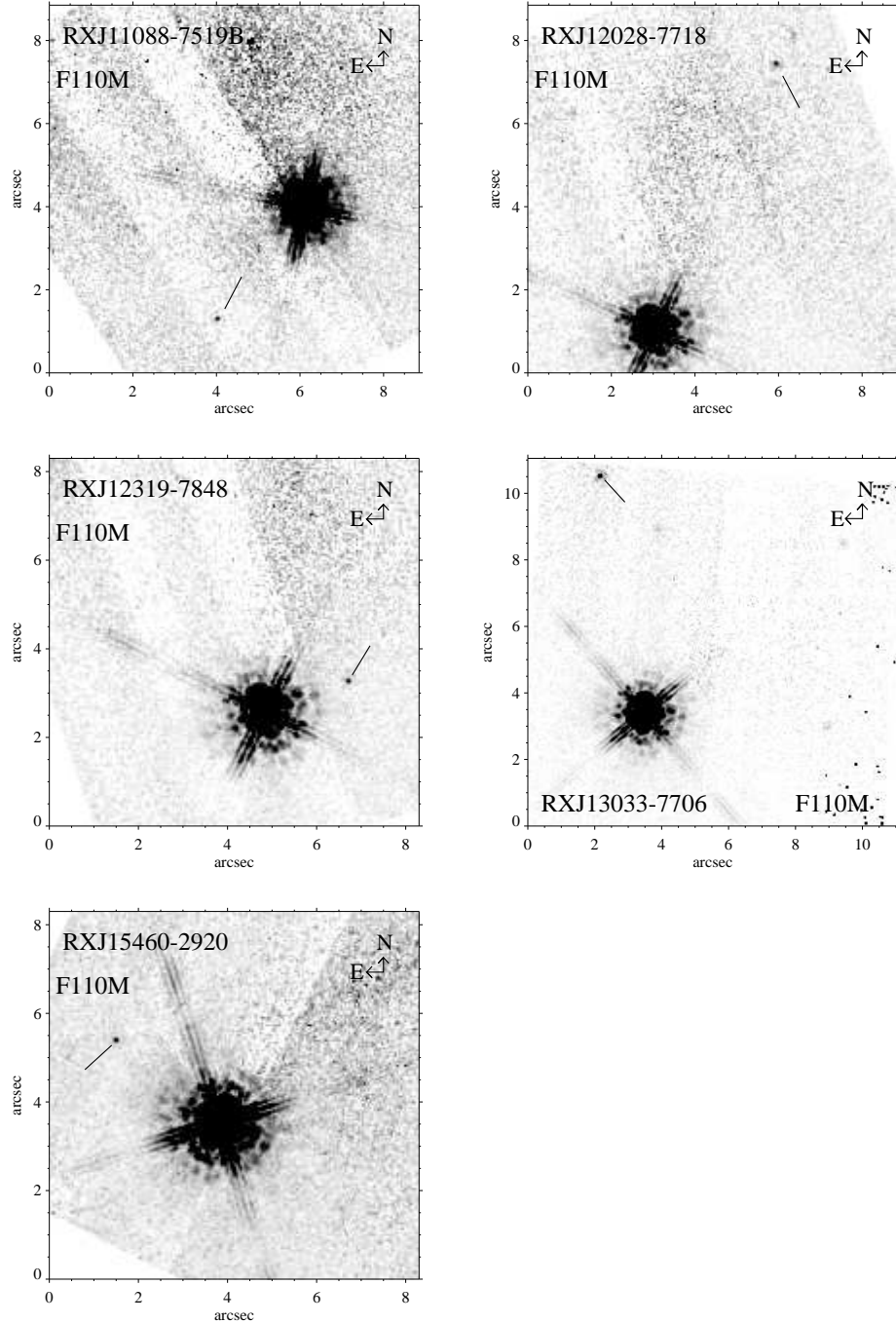


FIG. 2.— Faint field (background?) sources. North is up and east is to the left.

3.3.2. Observations and Data Reduction

The ISO observations with ISOCAM and ISOPHOT were carried out between 1997 Aug 04 and 24. Of the 30 WTTS and PTTS in the initial target list, only twelve were actually observed with ISOPHOT. The ISOPHOT observations of twelve stars were carried out as 3×3 maps using the PHT C100 detector in mode PHT22 and the C100_60_UM and C100_90_UM filters. NTTS155436-2313 was only observed with ISOPHOT. The other eleven stars were also observed with ISOCAM. The ISOCAM observations were obtained with a scale of $3''/\text{pixel}$ as 2×2

rasters using the LW2 ($6.75 \mu\text{m}$) and LW3 ($15 \mu\text{m}$) filters. No color information could be obtained for RXJ 15460-2920, as it was observed in LW2 only. Total exposure times were of the order of 200s to 240s per filter and object.

The data reduction was carried out using the software packages CAM Interactive Analysis and PHOT Interactive Analysis. The standard processing includes dark subtraction, deglitching, transient correction, flatfielding and mosaicing. None of the sources was detected at $60 \mu\text{m}$ and $90 \mu\text{m}$ down to a limiting flux of $\approx 400 \text{ mJy}$.

Figure 3 shows the pipeline reduced ISOCAM data in

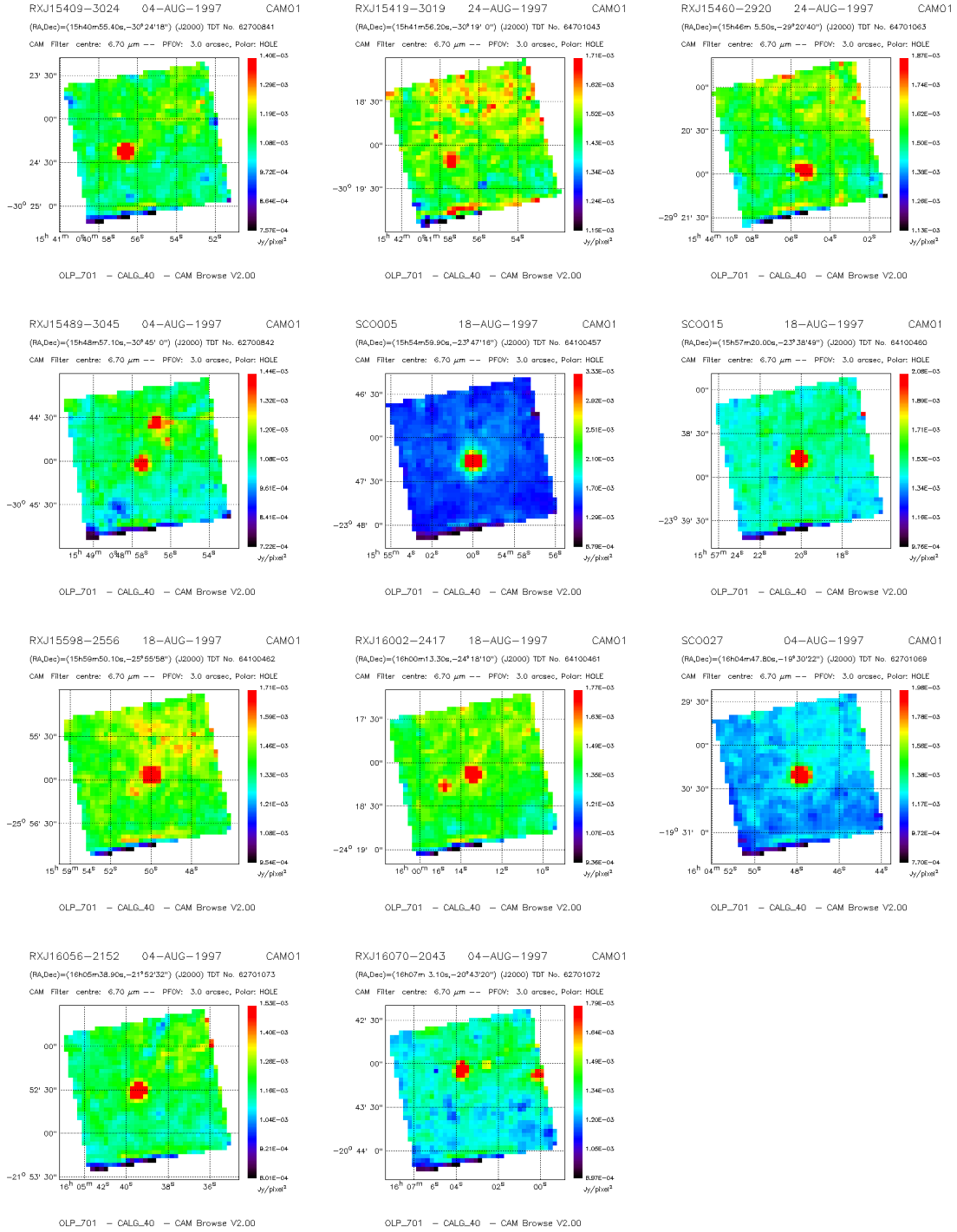


FIG. 3.— ISOCAM 6.75 μm observation of WTTs and PTTS in Scorpius-Centaurus. In addition to the target stars, photospheric emission from foreground stars has been detected in a number of cases. These foreground stars are brighter than the target stars in the optical, but considerably fainter in the infrared. North is up and east is to the left.

the LW2 filter. All eleven target stars (8 PTTS, 1 WTTs, 2 unclassified stars) are clearly detected (Moneti et al. 1999). On several occasions additional foreground (field) stars are also detected. Foreground stars can easily be distinguished from the WTTs and PTTS based on their LW3-LW2 colors (see below). Aperture photometry was performed using IRAF and 4.5 pixel and 5.5 pixel apertures for LW2 and LW3, respectively. Random uncertain-

ties should be of the order of a few percent, but systematic errors might be as large as 20% due to uncertainties in the transient correction and the uncertain color terms. Table 5 summarizes the results of the ISOCAM observations.

3.4. Ground-based NIR follow-up

Ground-based near-infrared spectroscopy of the target stars and the faint sources detected with HST/NICMOS

and adaptive optics was attempted in the course of two nights in April 1998 using the CTIO 4m Blanco telescope and the near infrared spectrograph. Due to fog and clouds, no useful data were obtained.

4. PHYSICAL COMPANIONS AND BACKGROUND SOURCES

4.1. Faint (Substellar?) Sources

The PSF subtraction of the HST/NICMOS data did not reveal any faint objects which would qualify as a candidate for a substellar companion within $2''$ of the WTTS and PTTS. A total of five point sources at projected separations $\gtrsim 2''$ and 6 to 8 mag fainter than their primary were detected in the 24 fields (Figure 2). Photometric and astrometric measurements for the faint sources are summarized in Table 4, and a plot of brightness difference between the primary and a possible companion vs. separation is shown in Figure 4.

The probability $P(\Theta, m)$ for an unrelated source to be located within a certain angular distance Θ from a particular target is given by

$$P(\Theta, m) = 1 - e^{-\pi\rho(m)\Theta^2} \quad (1)$$

where $\rho(m)$ is the cumulative surface density of background sources down to a limiting magnitude m . The probability for chance alignments increases with increasing angular distance and decreasing brightness. Therefore, in order to derive an estimate of $P(\Theta, m)$, one has to determine the local density of background sources first.

For the sources in Scorpius-Centaurus, parallel NIC2 observations of adjacent fields were obtained in the F110W

filter. The eleven NIC2 fields cover an area of about 4000 square arcsec. 68 sources with brightness values between $16^m.4$ and $23^m.2$ were detected. Figure 5 shows the cumulative brightness function $\rho(m)$ scaled to an area of 1 square degree. The number counts in the observed cumulative brightness function are in good agreement with the number counts expected according to the Galactic model by Wainscoat et al. (1992). No NIC2 parallel observations in F110W were obtained for the targets in Chamaeleon, but a cumulative brightness function can again be derived from the model by Wainscoat et al. (1992).

As the probability for physical association decreases with increasing angular separation, our best candidate for a true substellar companion is the faint source $\approx 2''$ northwest of RXJ12319-7848. According to equation (1) the bare-bone probability for it being an unrelated background source is only $\approx 5\%$. In other words, equation (1) yields a 95% probability for a physical association between the RXJ12319-7848/c and RXJ12319-7848. Similar reasoning has in the past frequently been cited as supporting evidence for the substellar nature of faint objects near a brighter star (e.g., 0918-0023B, Jones et al. 1994; TMR-1C, Terebey et al. 1998; TWA-7B, Neuhäuser et al. 2000a). In many cases, follow-up observations helped to establish the true nature of the faint object, and the object turned out to be an unrelated background star (e.g., TMR-1C, Terebey et al. 2000; TWA-7B, Neuhäuser et al. 2000b) or a distant galaxy (0918-0023B, Becklin et al. 1995).

It is therefore advisable to refrain from assigning probabilities to individual sources. Instead one should compute

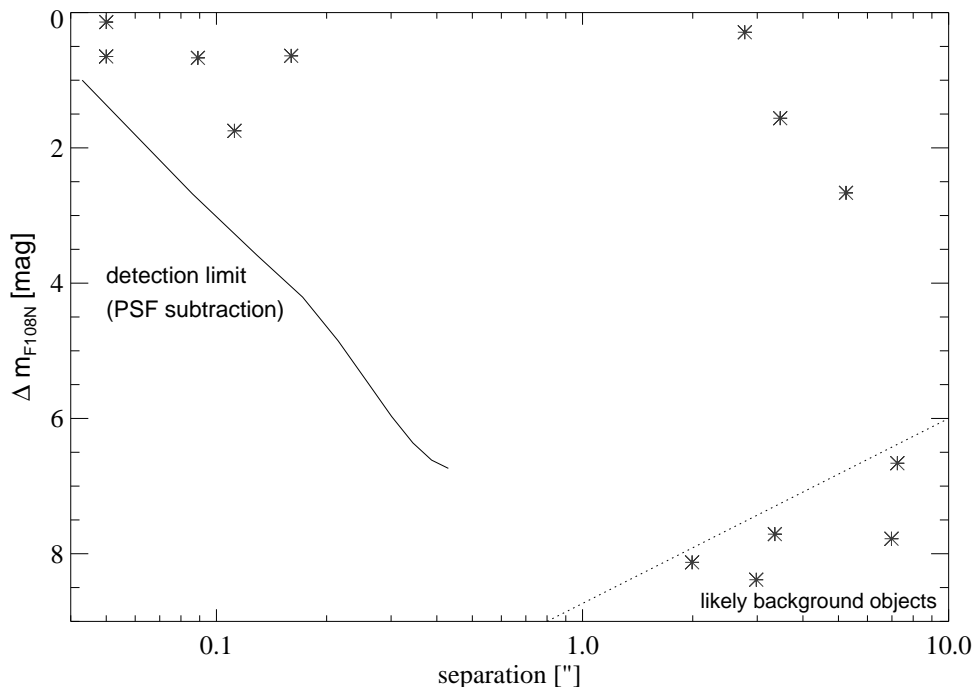


FIG. 4.— Distribution of the brightness difference between the target stars and their possible companions versus the angular separation. The solid line indicates the detection limit after PSF subtraction. It would have been possible to detect a $4^m.7$ fainter companion at a separation of $0''.2$ and an 8^m fainter companion at a separation of $1''$, but none were found. The region preferentially occupied by background objects is also shown (dotted line). Note that the lack of nearly equal brightness binaries with separation between $0''.2$ and $2''.5$ is due to the preselection against binaries identified in the ground-based speckle and direct imaging observations.

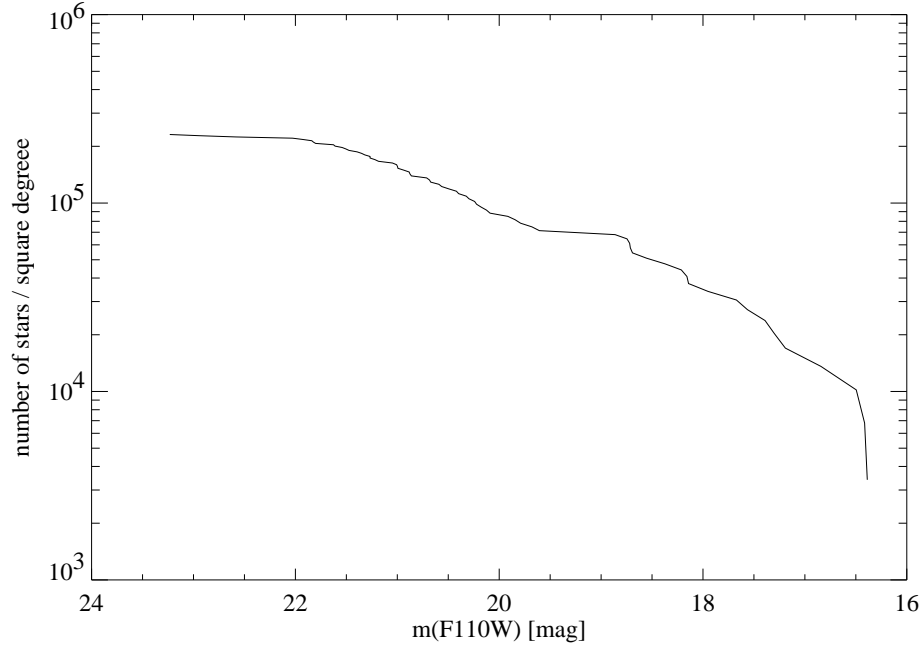


FIG. 5.— Background star counts as measured on the NIC2 parallel observations in the general direction of ScoCen ($l \approx 345^\circ$, $b \approx +15^\circ$) and scaled to 1 square degree. Based on these star counts, we expect on average 0.37 objects with $16^m75 \leq m_{F110M} \leq 19^m15$ per NIC1 frame, or 4.0 background sources in total on the 11 NIC1 frames towards ScoCen.

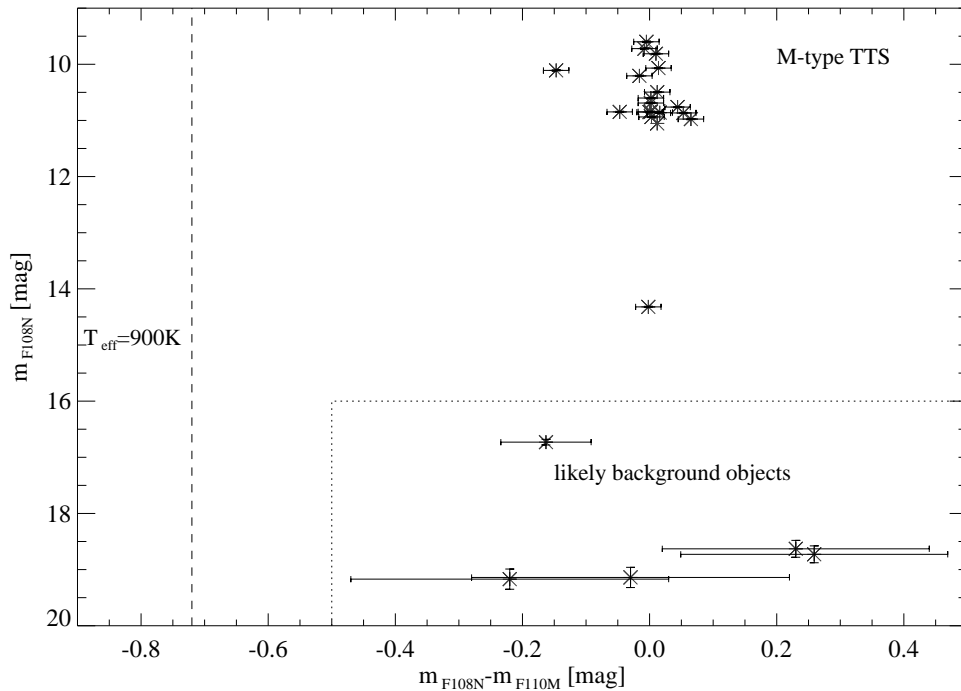


FIG. 6.— Color magnitude diagram for target stars (WTTS and PTTS) and faint sources. Most of the M-type TTS show $m_{F108N} - m_{F110M}$ colors close to 0 (with the exception of the PTTS RXJ 12046-7731). Because of their faintness, the colors of the suspected background objects have relatively large uncertainties, but all fall clearly outside the region occupied by substellar objects. The dashed line indicates the expected color for a brown dwarf with $T_{\text{eff}} = 900$ K.

the ensemble statistics. While the probability for finding a background object similar to RXJ12319-7848/c within $2''$ of RXJ12319-7848 is only 5%, the probability for finding any such object within $2''$ of one of the 24 HST/NICMOS

targets is $\approx 70\%$. It is thus not unlikely that RXJ12319-7848/c is an unrelated background source.

Based on the observed cumulative brightness function for Scorpius-Centaurus, one would expect to detect on av-

erage 4.0 sources with F110W magnitudes between 16^m75 and 19^m15 on the eleven NIC1 frames in the direction of Scorpius-Centaurus. One faint source was actually detected, which is a 1.5 sigma deviation from the expected average. According to the model by Wainscoat et al. (1992) 3.2 sources with J magnitudes between 16^m75 and 19^m15 would be expected on average in a field equivalent in size to the area covered by the 13 NIC1 frames. Four faint sources were detected on the NIC1 frames towards Chamaeleon, which is in good agreement with the theoretical expectation.

The agreement between the $m_{F108N} - m_{F110M}$ colors of the faint objects and the M-type WTTS and PTTS (Figure 6) provides additional evidence that the faint objects are unrelated background sources and not substellar companions.

4.2. Binary and multiple systems

In addition to 21 stars which were assumed to be single stars, also three wide binaries with separations $\geq 3''5$ were included in the sample. Three of the “single” stars turned out to be close binaries, and two of the three wide binaries turned out to be hierarchical triple systems (see Figure 1.). RXJ 11088-7519 constitutes an additional triple system, with RXJ 11088-7519a being a spectroscopic binary (Covino et al. 1997). The relatively high incidence of triple systems (see Figure 1) can be attributed to the selection effect in favor of multiple systems in ROSAT selected samples of young X-ray active late-type stars (see Brandner et al. 1996; Kunkel et al. 2000).

The adaptive optics observations led to the identification of two faint companions to X-ray active stars in Chamaeleon. The relatively small lithium equivalent widths of RXJ 12253-7857 and RXJ 14150-7822 (see Alcalá et al. 1997) indicates that both stars could be either pre-main-sequence stars with ages of up to 20 Myr or ZAMS stars. In all cases the brightness of the secondary suggests that it is a stellar companion (i.e., not substellar).

4.3. Implications

It seems likely that all five faint sources are background objects, and not physically related to the PTTS and WTTS. The lack of brown dwarf companions at separations larger than 30 A.U. ($0''2$ at 150 pc) indicates that wide brown dwarf companions are rare (less than 4% of all cases). This is in good quantitative agreement with the surveys for brown dwarf companions to white dwarfs (Probst 1983; Becklin & Zuckerman 1988) and M-dwarfs (Oppenheimer 1999; Burgasser et al. 2000) in the solar neighborhood. It implies that fragmentation of collapsing molecular cloud cores in general does not produce extremely unequal mass pairs. Alternatively, the density of circumstellar disks at radii greater than 30 A.U. appears to be too small to allow for the formation of massive substellar companions.

5. EVOLVED (REMNANT) CIRCUMSTELLAR DISKS

5.1. ISOCAM survey of low-mass star forming regions

A large scale ISOCAM survey of low-mass star forming regions in the solar neighborhood was carried out by Nordh and collaborators (Nordh et al. 1996, 1998; Olofsson et al. 1999; Persi et al. 1999). The first part of Nordh’s survey included the dark clouds Chamaeleon I,

Ophiuchus, Serpens, and Corona Australis and covered an area of 2.3 square degree. A total of 402 sources in Oph, Cha, and CrA were detected both in LW2 and LW3 (Nordh et al. 1998). When placed on a $\log F_{\nu}(\text{LW3})$ vs. $\log(F_{\nu}(\text{LW3})/F_{\nu}(\text{LW2}))$ magnitude-color diagram, the sources cluster in two distinctive groups. As discussed by Nordh et al. (1996), the two groups can be identified with disk-less main-sequence stars (stellar photospheres), and pre-main sequence stars with circumstellar disks.

The expected value of $R = \log \frac{F_{\nu}(\text{LW3})}{F_{\nu}(\text{LW2})}$ for disk-less main-sequence stars is approx. -0.68 and it is rather insensitive to the effective temperature of the star. For T Tauri stars with circumstellar disks, R can be derived from simple disk models. Kenyon & Hartmann (1995) computed the spectral index

$$\alpha_{12} = \frac{\log(\lambda_2 F_{\lambda_2}) - \log(\lambda_1 F_{\lambda_1})}{\log \lambda_2 - \log \lambda_1} \quad (2)$$

for flat and flared disk models. According to their models, $\alpha = -0.7$ for a flared disk and $\alpha = -1.3$ for a flat disk at $10 \mu\text{m}$. This corresponds to $R = -0.1$ and $R = +0.1$, respectively. About 90% of the 402 sources in the sample by Nordh et al. (1998) have either $R < -0.5$ or $R > -0.2$, and are thus either (disk-less) main-sequence stars or young pre-main sequence stars with circumstellar disks. Only about 10% of the sources fall in the transitional region with $-0.5 \leq R \leq -0.2$.

5.2. ISOCAM mini-survey of Scorpius-Centaurus

Our ISOCAM mini-survey in Scorpius-Centaurus covers only 10 stars (1 WTTS, 7 PTTS, and 2 unclassified stars) which were observed both with LW2 and LW3. Two stars (1 WTTS, 1 PTTS) have ISOPHOT observations, but no ISOCAM observations in LW3 (see Table 5). Figure 7 shows one of the above mentioned $\log F_{\nu}(\text{LW3})$ vs. $\log(F_{\nu}(\text{LW3})/F_{\nu}(\text{LW2}))$ magnitude-color diagrams for the sources detected towards Chamaeleon I by Nordh et al. (1996). Overplotted are the sources from the present survey. Interestingly, the majority of the stars in our sample (seven out of ten) have R in the range of -0.2 to -0.5 , whereas the large majority of the sources in Chamaeleon and other low-mass star forming regions have R values outside this range. The values of R measured for our sample of PTTS are on average higher than the values for a pure stellar photosphere, but significantly less than the typical value measured for CTTS and WTTS in low-mass star forming regions.

5.3. Implications

The non-detection with ISOPHOT at $60 \mu\text{m}$ and $90 \mu\text{m}$ confirms the absence of cold, massive dust disks around the low-mass WTTS and PTTS in ScoCen. The ISOCAM observations, however, indicate the presence of circumstellar material (presumably in form of a circumstellar disk). The physical properties of the disks in ScoCen appear to be different from the disks typically found around CTTS and WTTS in low-mass star forming regions. The difference in R (or spectral index α) can be explained by differences in the global dust opacities at $6.5 \mu\text{m}$ and $15 \mu\text{m}$ in both types of disks.

Suttner, Yorke & Lin (1999) studied dust coagulation in the envelopes around young stellar objects. They simulated the effect of grain size on the specific extinction

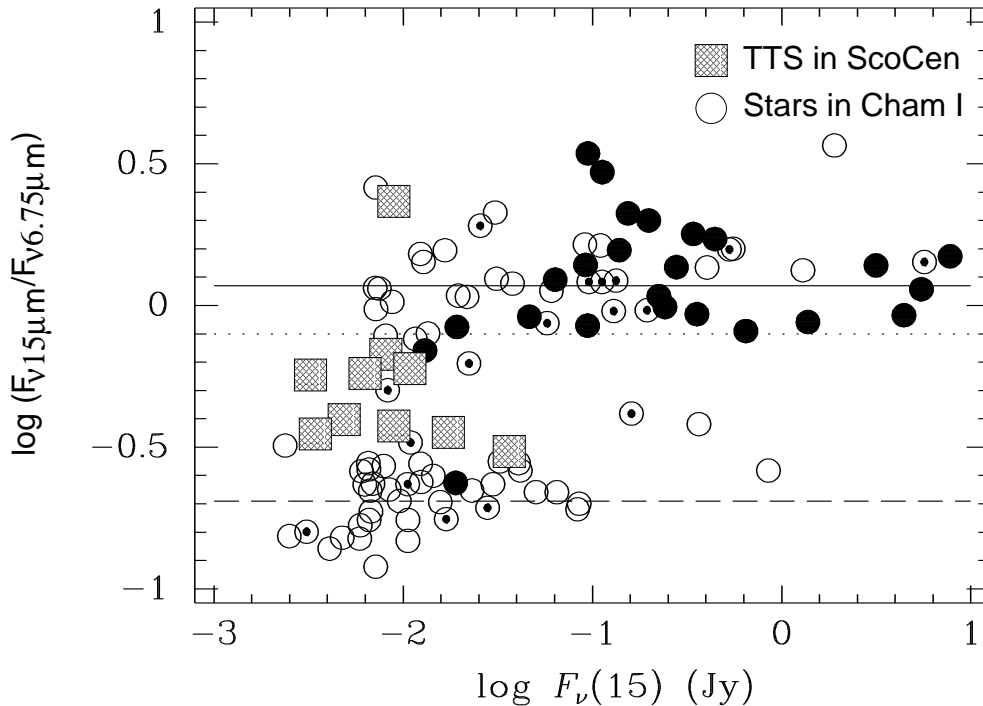


FIG. 7.— (adapted from Nordh et al. 1996) Color-magnitude diagram based on ISOCAM observations of young stars in Chamaeleon (circles) and Scorpius-Centaurus (squares). Black filled circles indicate previously known YSOs and CTTSs, circles with a central dot previously known WTTS, and open circles new sources detected with ISO by Nordh et al. (1996). The dashed line indicates the location of pure stellar photospheres, the dotted and solid line the location of flat and flared circumstellar disks, respectively, as predicted by the models from Kenyon & Hartmann (1995). WTTS and PTTS in ScoCen show a spectral index intermediate between main-sequence stars and CTTS and WTTS in Chamaeleon.

coefficient. Figure 1 in their paper indicates that a change in the average dust grain size from $0.1 \mu\text{m}$ to $5 \mu\text{m}$ leads to an increase of the specific extinction coefficient κ_i^{ext} at $6.5 \mu\text{m}$ by a factor of ≈ 5 , whereas κ_i^{ext} at $15 \mu\text{m}$ remains virtually unchanged. Such an increase in $\kappa_i^{\text{ext}}(6.5 \mu\text{m})$ is equivalent to an increase in the spectral index α . A “flat” spectral index $\alpha = 0$, e.g., corresponds to $R = -0.35$. Thus any mechanism which preferentially removes or destroys smaller grains can provide a viable explanation for the observed differences in the spectral index of PTTS in ScoCen and WTTS and CTTS in low-mass starforming regions such as Chamaeleon.

The higher ratio of PTTS to WTTS in Scorpius-Centaurus compared to Chamaeleon suggests that the X-ray active low-mass stars in Scorpius-Centaurus are on average older than their counterparts in Chamaeleon. Alcalá et al. (1997) assign ages less than 5 Myr to the majority of the X-ray active stars in Chamaeleon, whereas Kunkel et al. (2000) find average ages in the range of 5 to 15 Myr for the WTTS and PTTS in Scorpius-Centaurus. Disk evolution and grain growths in circumstellar disks would lead to a deficiency in smaller grains. Such a deficiency in smaller grains should only last until a critical number of massive particles like rocks and planetesimals has formed. Collisions between individual planetesimals will then replenish the disk with smaller grains. During the initial build-up period, however, there should be a phase in which a disk

is almost devoid of smaller grains.

Apart from the age difference, the PTTS in ScoCen are located in an OB association, and thus – unlike the WTTS and CTTS in T-associations – subject to the effects of nearby O stars and supernova explosions. Both impacting shock fronts (Dwek et al. 1996) and high energy photons from nearby O stars and occasional supernova explosions (Voit 1991) could change the distribution of grain sizes. Overall, however, the contribution of Lyman continuum radiation to dust destruction should be negligible as only grains with sizes of $\lesssim 0.001 \mu\text{m}$ are affected (see discussion in Richling & Yorke 1997).

Thus disk evolution appears to be the more likely explanation for the difference in spectral index between CTTS and WTTS in Chamaeleon and the PTTS in Scorpius-Centaurus.

6. SUMMARY

High-spatial resolution HST and ground-based adaptive optics observations, and high-sensitivity ISO (ISOCAM & ISOPHOT) observations of a sample of X-ray selected weak-line (WTTS) and post (PTTS) T Tauri stars located in the nearby Chamaeleon T and Scorpius-Centaurus OB associations were obtained and analyzed.

The HST/NICMOS and adaptive optics observations aimed at identifying substellar companions (young brown dwarfs) at separations ≥ 30 A.U. ($0''.2$ at 150 pc) from the

primary stars. While the sample was preselected against binary stars with $0''.2 < \text{sep.} < 3''$, we detected 5 binary stars with separations $< 0''.2$. The largest brightness difference between a primary and a secondary in these close binaries is $1^m.75$. The relatively small brightness difference indicates that all five secondaries at separations $< 0''.2$ are low-mass stars with masses clearly above the hydrogen burning limit. Even though it would have been possible to detect a $4^m.7$ fainter object at a separation of $0''.2$ from the primary star, or a 8^m fainter object at a separation $\geq 1''$ from the primary star, no such objects were found within 300 A.U. ($2''$) of any of the target stars. 5 objects at separations larger than $2''$, and 6 mag to 8 mag fainter than the target stars can very likely be attributed to a population of field (background) stars. We conclude that the formation of massive substellar companions at separations larger than 30 A.U. from the primary star is very unlikely.

ISOCAM observations of WTTS and PTTS in ScoCen reveal infrared excesses which are clearly above photospheric levels, and which have a spectral index intermediate between that of younger (1 to 5 Myr) T Tauri stars in Chamaeleon and that of pure stellar photospheres. The difference in the spectral index of the older WTTS and PTTS in ScoCen compared to the younger classical and weak-line TTS in Cha can be understood in terms of disk evolution, and could hint that circumstellar disks start to get dust depleted at an age of around 5 to 15 Myr. Dust depletion is very likely related to the build-up of larger particles (ultimately rocks and planetesimals) and thus an indicator for the onset of the period of planet formation.

In evolved disks, the presence of larger grains resulting from dust coagulation and the gradual build-up of larger

bodies should manifest itself both in the scattering properties at longer wavelengths and in spectral features. In the near future, using SIRTF/IRS and SOFIA, it will become possible to study the mid- and far-infrared properties of the circumstellar disks around the PTTS in ScoCen and other nearby star forming regions. Furthermore, high-sensitivity CO surveys with the Atacama Large Millimeter Array will be able to detect also the gaseous component of the disks around the PTTS and WTTS in ScoCen and Chamaeleon. These surveys will provide the final answer to the question whether massive gaseous disks can survive long enough to allow for slow accretion of gas onto proto-giant planets over timescales of 10^7 yr, or if giant planets have to form on much shorter time scales by disk instabilities.

Support for this work was provided by NASA through grant number GO-07412.01-96A from the Space Telescope Science Institute, which is operated by the Association of Universities for Research in Astronomy, Inc., under NASA contract NAS5-26555. This publication makes use of data products from 2MASS, which is a joint project of UMass and IPAC/Caltech, funded by NASA and NSF. We would like to thank the program coordinator Chris Ready and the contact scientist Keith Noll for their help in implementing the HST observing program, and Dan Potter for providing the numbers of the theoretical background source density. WB acknowledges support by You-Hua Chu and Deborah L. Padgett, and by the National Science Foundation. AS acknowledges support from the Deutsche Forschungsgemeinschaft (DFG) under grant 1053/8-1 and NASA ATP grant NAG 5-8425 to the University of Georgia.

REFERENCES

- Alcalá, J.M., Krautter J., Schmitt, J. H. M. M., Covino E., Wichmann R., Mundt R. 1995, *A&AS*, 114, 109
 Alcalá, J.M., Krautter J., Covino E., Schmitt, J.H.M.M., Wichmann R., 1997, *A&A*, 319, 184
 Allard, F., Hauschildt, P.H. 1995, *ApJ* 445, 433
 Allard, F., Hauschildt, P.H., Alexander, D.R., Starrfield, S. 1997, *ARA&A* 35, 137
 Allard, F., Hauschildt, P.H., Baraffe, I., Chabrier, G. 1996, *ApJ* 465, L123
 Artymowicz, P., Lubow, S.H. 1994, *ApJ* 421, 651
 Baraffe, I., Chabrier, G., Allard, F., Hauschildt, P.H. 1998, *A&A* 337, 403
 Becklin, E., Zuckerman, B. 1988, *Nature* 336, 656
 Becklin, E., Macintosh, B., Zuckerman, B. 1995, *ApJ* 449, L117
 Beckwith, S.V.W., Sargent, A.I., Chini, R.S., Guesten, R. 1990, *AJ*, 99, 924
 Bodenheimer, P. 1965, *ApJ*, 142, 451
 Boss, A.P. 1998, *ApJ*, 503, 923
 Brandner, W., Alcalá, J. M., Kunkel, M., Moneti, A., Zinnecker, H. 1996, *A&A*, 307, 121
 Brandner W., Zinnecker H., Allard, F. 1997, in "Brown Dwarfs and Extrasolar Planets", eds. R. Rebolo et al., ASP Conf. Ser. 134, p. 288
 Brandner, W., Köhler, R. 1998, *ApJ* 499, L79
 Burgasser, A.J., Kirkpatrick, D., Cutri, R.M., McCallon, H., Kopan, G. et al. 2000, *ApJ Letters*, in press
 Burrows, C.J., Stapelfeldt, K.R., Watson, A.M., Krist, J.E., Ballester, G.E. et al. 1996, *ApJ* 473, 437
 Burrows, A., Marley, M., Hubbard, W.B., Lunine, J.I., Guillot, T. et al. 1997, *ApJ* 491, 856
 Césarsky, C.J., Abergel, A., Agnèsè, P. et al. 1996, *A&A* 315, L32
 Covino, E., Alcalá, J.M., Allain, S., Bouvier, J., Terranegra, L., Krautter, J. 1997, *A&A*, 328, 187
 Dwek, E., Foster, S.M., Vancura, O. 1996, *ApJ* 457, 244
 Feigelson, E.D. 1996, *ApJ* 468, 306
 Frink, S., Röser, Neuhäuser, R., Sterzik, M.F. 1997, *A&A* 325, 613
 Frink, S., Röser, S., Alcalá, J.M., Covino, E., Brandner, W. 1998, *A&A* 338, 442
 Hauschildt, P.H., Allard, F., Ferguson, J., Baron, E., Alexander, D.R. 1999, *ApJ* 525, 871
 Henning, T., Pfau, W., Zinnecker, H., Prusti, T. 1993, *A&A* 276, 129
 Herbig, G.H. 1965, *ApJ*, 141, 588
 Jones, H.R.A., Miller, L., Glazebrook, K. 1994, *MNRAS* 270, L47
 Kant, I. 1755, *Allgemeine Naturgeschichte und Theorie des Himmels*, Leipzig
 Kenyon, S.J., Hartmann, L. 1995, *ApJS* 101, 117
 Kessler, M.F., Steinz, J.A., Anderegg, M.E., Clavel, J., Drechsel, G. et al. 1996, *A&A* 315, L27
 Köhler, R., Kunkel, M., Leinert, Ch., Zinnecker, H. 2000, *A&A*, in press
 Koresko, C.D. 1998, *ApJ* 507, L145
 Krist, J., Hook, R. 1997, *The Tiny Tim User's Handbook*, Version 4.4, Baltimore:STScI
 Kunkel, M., Brandner, W., Yorke, H.W., Zinnecker, H., Neuhäuser, R., Schmitt, J.H.M.M., Mayor, M., Udry, S. 2000, *ApJ Supp.*, submitted
 Lemke, D., Klaas, U., Abolins, J. et al. 1996, *A&A* 315, L64
 Lissauer, J.J. 1987, *Icarus*, 69, 249
 Malkov, O., Piskunov, A., Zinnecker, H. 1998, *A&A* 338, 452
 Marcy, G.W., Butler, R.P. 1996, *ApJ*, 464, L147
 Martín, E.L., 1997, *A&A*, 321, 492
 Martín, E.L., 1998, *AJ*, 115, 351
 Mayor, M., Queloz, D. 1995, *Nature*, 378, 355
 McCaughrean, M.J., O'Dell, C.R. 1996, *AJ*, 111, 1977
 Miller, G.E., Scalo, J.M. 1978 *PASP* 90, 506
 Moneti, A., Zinnecker, H., Brandner, W., Wilking, B. 1999, in "Astrophysics with Infrared Surveys: A Prelude to SIRTF", ASP Conf. Series 117, eds. M.D. Bica, C.A. Beichman, R.M. Cutri, B.F. Madore, p. 355
 Monin, J.-L., Bouvier, J. 2000, *A&A* 356, L75
 Neuhäuser, R., Brandner, W. 1998, *A&A*, 330, L29
 Neuhäuser, R., Brandner, W., Eckart, A., Guenther, E., Alves, J., Ott, Th., Huelamo, N., Fernandez, M. 2000a, *A&A*, 354, L9
 Neuhäuser, R. et al., 2000b, in prep.

- Nordh, L., Olofsson, G., Abergel, A., Andre, P., Blommaert, J. et al. 1996, *A&A Letters* 315, 185
- Nordh, L., Olofsson, G., Bontemps, S., Hultgren, M., Kaas, A.A. et al. 1998, in *Star Formation with the Infrared Space Observatory*, eds. Joao Yun & Rene Liseau, ASP 132, p. 127
- O'Dell, C.R.O., Wen, Z., Hu, X. 1993, *ApJ*, 410, 686
- Olofsson, G., Hultgren, M., Kaas, A.A., Bontemps, S., Nordh, L. et al. 1999, *A&A* 350, 883
- Oppenheimer, B.R. 1999, PhD thesis, Caltech, Pasadena, CA
- Papaloizou, J., Pringle, J.E. 1977, *MNRAS* 181, 441
- Persi, P., Marenzi, A.R., Kaas, A.A., Olofsson, G., Nordh, L., Roth, M. 1999, *AJ* 117, 439
- Probst, R. 1983 *ApJ* 274, 237
- Richling, S., Yorke, H.W. 1997, *A&A* 327, 217
- Stapelfeldt, K.R., Krist, J.E., Menard, F., Bouvier, J., Padgett, D.L., Burrows, C.J. 1998, *ApJ* 502, L65
- Suttner, G., Yorke, H.W., Lin, D.N.C. 1999, *ApJ* 524, 857
- Terebey, S., van Buren, D., Padgett, D.L., Hancock, T., Brundage, M. 1998, *ApJ* 507, L71
- Terebey, S., van Buren, D., Matthews, K., Padgett, D.L. 2000, *AJ*, in press (May issue)
- Thompson, R.I., Rieke, M., Schneider, G., Hines, D.C., Corbin, M.R. 1998, *ApJ* 492, L95
- Vanhalla, H.A.T. 1998, *Proc. Indian Acad. Sci. (Earth Planet Sci.)* 107, 391
- Voit, G.M. 1991, *ApJ* 379, 122
- Wainscoat, R.J., Cohen, M., Volk, K., Walker, H.J., Schwartz, D.E. 1992, *ApJS* 83, 111
- Walter, F.M., Vrba, F.J., Mathieu, R.D., Brown, A., Myers, P.C. 1994, *AJ*, 107, 692

TABLE 1

The expected brightness difference in various NIC1 filters between an M-type primary with an effective temperature of 2800K (M6) or 3800K (M0), respectively, and a young brown dwarf with $T_{\text{eff}}=900\text{K}$. F145M and F165M provide color information, albeit at worse spatial resolution than F108N. For comparison, the expected brightness difference in the WFPC2 F1042M filter is shown.

Filter	$\Delta m_{T2800K/T900K}$ [mag]	$\Delta m_{T3800K/T900K}$ [mag]
F095N	7.9	9.3
F097N	7.8	9.2
F108N	5.2	6.2
F113N	8.9	9.9
F164N	6.0	6.9
F166N	5.5	6.5
F187N	8.5	10.0
F090M	7.6	9.1
F110M	5.9	7.0
F145M	7.0	8.2
F165M	5.1	6.1
F170M	5.8	6.9
F110W	5.6	6.7
F140W	5.5	6.6
F160W	5.6	6.7
WFPC2:		
F1042M	6.1	7.4

TABLE 2

Target List. Coordinates are presented in columns 2 and 3. Column 4 lists whether the object has been observed with HST or ISO. Column 5 list aliases when available.

Target	$\alpha(2000)$ [hms]	$\delta(2000)$ [$^{\circ}$ ' '']	HST/ISO obs.	Alias
RXJ08480-7854 ¹	08 47 57.21	-78 54 54.0	HST	
RXJ09029-7759 ¹	09 02 51.85	-77 59 35.2	HST	
RXJ10053-7749 ¹	10 05 20.54	-77 48 42.8	HST	
RXJ11088-7519B ¹	11 08 52.92	-75 19 03.1	HST	
RXJ11498-7850 ¹	11 49 32.60	-78 51 00.7	HST	
RXJ11585-7754B ¹	11 58 27.57	-77 54 44.8	HST	
RXJ12028-7718 ¹	12 02 55.25	-77 18 37.7	HST	
RXJ12046-7731 ¹	12 04 36.78	-77 31 34.2	HST	
RXJ12077-7953 ¹	12 07 48.96	-79 52 42.3	HST	
RXJ12197-7403 ¹	12 19 44.24	-74 03 56.9	HST	
RXJ12319-7848 ¹	12 31 56.61	-78 48 32.0	HST	
RXJ12436-7834 ¹	12 43 37.21	-78 34 07.4	HST	
RXJ13033-7706 ¹	13 03 04.84	-77 07 02.0	HST	
RXJ15241-3030B ²	15 24 12.99	-30 30 56.0	HST	
RXJ15409-3024 ²	15 40 56.50	-30 24 23.3	HST, ISO	
RXJ15419-3019 ²	15 41 57.49	-30 19 04.5	HST, ISO	
RXJ15438-3306 ²	15 43 51.58	-33 06 29.4	HST	
RXJ15460-2920 ²	15 46 05.26	-29 20 52.1	HST, ISO	
RXJ15489-3045 ²	15 48 57.30	-30 45 02.4	HST, ISO	
RXJ15549-2347 ^{2,3}	15 54 59.9	-23 47 18	ISO	Sco005
NTTS155421-2330 ³	15 57 20.0	-23 38 49	ISO	Sco015
NTTS155436-2313 ³	15 57 34.4	-23 21 11	ISO	Sco017
RXJ15598-2556 ²	15 59 50.05	-25 55 57.9	HST, ISO	
RXJ16002-2417 ²	16 00 13.32	-24 18 10.2	HST, ISO	
RXJ16043-2130B ²	16 04 21.07	-21 30 41.9	HST	
RXJ16047-1930 ^{2,3}	16 04 47.8	-19 30 23	ISO	Sco027
RXJ16056-2152 ²	16 05 39.40	-21 52 34.0	HST, ISO	
RXJ16070-2043 ²	16 07 03.75	-20 43 07.3	HST, ISO	

¹Alcalá et al. 1995, 1997; ²Kunkel et al. 2000; ³Walter et al. 1994

TABLE 3

Physical Parameters: Spectral type, Lithium equivalent width, V magnitude and V-J color are from Alcalá et al. (1995, 1997), Kunkel et al. (2000) and Walter et al. (1994), except where mentioned otherwise.

Target	TTS-class	SpT	EW(Li) [Å]	V [mag]	V-J [mag]	m _{F108N} [mag]	m _{F108N} -m _{F110M} [mag]	F _ν (F108N) [mJy]
RXJ08480-7854	W	M2	0.61	13.19	3.89	9.60	-0.005	296.5
RXJ09029-7759	P	M3	0.50	13.99	...	10.50	0.012	129.8
RXJ10053-7749	W	M1	0.57	13.41	3.59	10.21	-0.016	169.5
RXJ11088-7519B	P	M3	0.50	14.78	...	10.97	0.065	83.7
RXJ11498-7850	P	M1	0.50	14.37	...	9.81	0.010	243.4
RXJ11585-7754B	W	M3	0.60	14.29	3.97	10.69	0.002	108.6
RXJ12028-7718	W	M0	0.60	14.38	...	10.85	0.000	93.5
RXJ12046-7731	P	M2	0.47	13.78	...	10.11	-0.147	185.3
RXJ12077-7953	W	M4	0.60	14.52	...	10.85	0.002	94.9
RXJ12197-7403	W	M0	0.56	13.12	...	10.09	...	189.5
RXJ12319-7848	W	M1	0.60	14.17	3.90	10.60	0.002	117.8
RXJ12436-7834	W	M0	0.70	13.13	3.75	9.72	-0.008	265.0
RXJ13033-7706	W	K7/M0	0.60	13.23	...	10.07	0.01	192.5
RXJ15241-3030B	P	M1	0.38	13.58	...	10.95	...	85.8
RXJ15409-3024	P	M2	0.11	14.53	3.89 ¹	11.02	...	80.2
RXJ15419-3019	P	M4	0.19	16.06	4.29 ¹	12.18	...	27.6
RXJ15438-3306S	?	M3	0.04	14.86	4.20	11.56	...	48.6
RXJ15438-3306N	11.85	...	37.2
RXJ15460-2920	P	M0	0.42	13.46	...	10.76	0.044	101.6
RXJ15489-3045	P	M2	0.09	15.28	4.03 ¹	11.66	...	44.5
RXJ15549-2347	?	G2	0.28	8.93	1.36
NTTS155421-2330	P	M0	0.28	12.78	3.09
NTTS155436-2313	W	M0	0.58	13.63	3.77
RXJ15598-2556A	P	M2	0.31	14.21	3.61	10.94	0.003	86.4
RXJ15598-2556BC	14.32	-0.002	3.8
RXJ16002-2417	P	M0	0.47	13.66	3.20 ¹	10.87	0.053	92.2
RXJ16043-2130B	P	M2	0.38	15.06	4.62	10.85	-0.047	93.9
RXJ16047-1930	?	K3	0.32	11.17	2.25
RXJ16056-2152	P	M1	0.50	14.26	...	10.86	0.016	92.7
RXJ16070-2043	W	M1	0.55	14.51	...	11.05	0.012	77.6

¹J magnitudes based on 2MASS Second Incremental Release data products.

TABLE 4

Separation, position angle, and photometric measurements for components of multiple systems and faint field (background?) sources

Target	separation ["]	PA [°]	m_{F108N} [mag]	$m_{F108N}-m_{F110M}$ [mag]	$F_\nu(F108N)$ [mJy]
RXJ11088-7519Ba	11.45	0.065	53.7
RXJ11088-7519Bb	0.160±0.010	2.8±0.4	12.08	0.065	30.0
RXJ12436-7834a	10.39	-0.04:	140.0
RXJ12436-7834b	0.05:	155.3±1.8	10.53	0.02:	123.0
RXJ15241-3030Ba	10.94	...	84.9
RXJ15241-3030Bb	3.467	300.5±0.1	12.52	...	19.7
RXJ15438-3306Na	12.03	...	30.9
RXJ15438-3306Nb	0.05:	17.8:	12.68	...	17.0
RXJ15598-2556Ca	14.53	-0.03	3.0
RXJ15598-2556Cb	0.112±0.005	211.0±0.3	16.28	0.08	0.60
RXJ16043-2130Ba ¹	11.38	0.02	56.5
RXJ16043-2130Bb ¹	0.089±0.005	342.5±0.2	12.05	0.02	30.5
RXJ11088-7519B/c	3.352±0.030	142.44±0.39	19.16±0.18	-0.22±0.25	0.04
RXJ12028-7718/c	6.980±0.008	335.69±0.01	18.63±0.15	0.23±0.21	0.07
RXJ12319-7848/c	1.992±0.002	290.83±0.14	18.73±0.15	0.26±0.21	0.07
RXJ13033-7706/c	7.243±0.002	10.19±0.01	16.73±0.05	-0.16±0.07	0.42
RXJ15460-2920/c	2.928±0.021	50.37±0.31	19.15±0.18	-0.03±0.25	0.05

¹Comparison to Köhler et al. (2000) indicates that RXJ16043-2130B rotates counterclockwise with a rate of approx. 5° yr⁻¹.

TABLE 5

Flux values derived from ISOCAM observations for 8 PTTS, 2 WTTS, and 2 unclassified stars. The unclassified star RXJ 15549-2347 (Sco005), which is the only G-type star in the sample, is also the only star with $R < -0.5$, and thus very likely a disk-less main-sequence star. Two stars have $R > -0.2$. RXJ 15598-2556 is a triple system which is unresolved by ISO. RXJ 15419-3019 has a spectral type of M4.

Target	$F_\nu(6.75 \mu\text{m})$ [mJy]	$F_\nu(15 \mu\text{m})$ [mJy]	R	TTS class	Alias
RXJ15409-3024	12.5	4.5	-0.45	P	
RXJ15419-3019	4.4	11.7	+0.42	P	
RXJ15460-2920	11.3	P	
RXJ15489-3045	6.9	3.8	-0.26	P	
RXJ15549-2347	114.7	32.8	-0.54	?	Sco005
NTTS155421-2330	24.4	9.6	-0.40	P	Sco015
NTTS155436-2313	W	Sco017
RXJ15598-2556	14.5	9.6	-0.18	P	
RXJ16002-2417	14.4	9.1	-0.20	P	
RXJ16047-1930	49.2	16.9	-0.46	?	Sco027
RXJ16056-2152	15.9	7.2	-0.34	P	
RXJ16070-2043	14.0	7.5	-0.27	W	